

Learning Chemical Reaction Representation with Reactant-Product Alignment

Kaipeng Zeng

MoE Key Laboratory of Artificial Intelligence, AI Institute, Shanghai
Jiao Tong University
Shanghai, China

Xianbin Liu

MoE Key Laboratory of Artificial Intelligence, AI Institute, Shanghai
Jiao Tong University
Shanghai, China

Yu Zhang

MoE Key Laboratory of Artificial Intelligence, AI Institute, Shanghai
Jiao Tong University
Shanghai, China

Xiaokang Yang

MoE Key Laboratory of Artificial Intelligence, AI Institute, Shanghai
Jiao Tong University
Shanghai, China

Yaohui Jin

MoE Key Laboratory of Artificial Intelligence, AI Institute, Shanghai
Jiao Tong University
Shanghai, China

Yanyan Xu

MoE Key Laboratory of Artificial Intelligence, AI Institute, Shanghai
Jiao Tong University
Shanghai, China

Abstract

Organic synthesis stands as a cornerstone of chemical industry. The development of robust machine learning models to support tasks associated with organic reactions is of significant interest. However, current methods rely on hand-crafted features or direct adaptations of model architectures from other domains, which lacks feasibility as data scales increase or overlook the rich chemical information inherent in reactions. To address these issues, this paper introduces RAlign, a novel chemical reaction representation learning model tailored for a variety of organic-reaction-related tasks. By integrating atomic correspondence between reactants and products, our model discerns the molecular transformations that occur during the reaction, thereby enhancing the comprehension of the reaction mechanism. We have designed an adapter structure to incorporate reaction conditions into the chemical reaction representation, allowing the model to handle diverse reaction conditions and adapt to various datasets and downstream tasks, e.g., reaction performance prediction. Additionally, we introduce a reaction-center aware attention mechanism that enables the model to concentrate on key functional groups, thereby generating potent representations for chemical reactions. Our model has been evaluated on a range of downstream tasks, including reaction condition prediction, reaction yield prediction, and reaction selectivity prediction. Experimental results indicate that our model markedly outperforms existing chemical reaction representation learning architectures across all tasks. Notably, our model significantly outperforms all the baselines with up to 25% (top-1) and 16% (top-10) increased accuracy over the strongest baseline on USPTO_CONDITION dataset for reaction condition prediction. We plan to open-source the code contingent upon the acceptance of the paper.

CCS Concepts

• Applied computing → Chemistry; • Computing methodologies → Artificial intelligence.

Keywords

Chemical Reaction Representation, Reaction Condition Prediction, Reaction Yield Prediction, Reaction Selectivity Prediction

ACM Reference Format:

Kaipeng Zeng, Xianbin Liu, Yu Zhang, Xiaokang Yang, Yaohui Jin, and Yanyan Xu. 2018. Learning Chemical Reaction Representation with Reactant-Product Alignment. In *Proceedings of Make sure to enter the correct conference title from your rights confirmation email (Conference acronym 'XX)*. ACM, New York, NY, USA, 13 pages. <https://doi.org/XXXXXXX.XXXXXXX>

1 Introduction

Organic synthesis has long been an essential component of the organic chemical industry, particularly within the pharmaceutical sector. Despite advancements in chemical synthesis technology, a range of tasks related to organic reactions remain challenging for humans, such as retrosynthesis planning and reaction condition recommendation. With the growth in computing power, data availability, and AI techniques, various models have been developed for organic chemistry, including graph-based [28, 39] and sequence-based [17] models. However, current research mainly concentrates on molecular representation learning, and there is still a deficiency in effective reaction representation to tackle the relation of molecules during the complex reaction process. This work focuses on the backbone design for chemical reaction representation learning, with the aim of improving this situation.

Existing chemical reaction representation learning methods can be roughly classified into two groups: fingerprint-based and deep-learning based. fingerprint-based methods use hand-craft fingerprints as molecular representations. These methods [38, 41] employ various strategies to integrate the molecular representations of different components of a chemical reaction to derive a comprehensive chemical reaction representation. The representations are usually combined with conventional machine learning models, such as XGBoost [6], to tackle downstream tasks. While these approaches do not necessitate extensive computational resources and have proven

Permission to make digital or hard copies of all or part of this work for personal or classroom use is granted without fee provided that copies are not made or distributed for profit or commercial advantage and that copies bear this notice and the full citation on the first page. Copyrights for components of this work owned by others than the author(s) must be honored. Abstracting with credit is permitted. To copy otherwise, or republish, to post on servers or to redistribute to lists, requires prior specific permission and/or a fee. Request permissions from permissions@acm.org.
Conference acronym 'XX, June 03–05, 2018, Woodstock, NY

© 2018 Copyright held by the owner/author(s). Publication rights licensed to ACM.
ACM ISBN 978-1-4503-XXXX-X/18/06
<https://doi.org/XXXXXXX.XXXXXXX>

effective with limited datasets, they may encounter performance limitations when scaling to larger datasets and more complex scenarios. This is attributed to the oversimplification of information inherent in the manually designed, statistically based features.

Working towards more powerful chemical reaction representations, researchers have increasingly turned to deep learning techniques. Leveraging SMILES [52], chemical reactions can be encoded into a string format, allowing the application of natural language processing methodologies to address the challenge of chemical reaction representation learning [31, 44]. Some studies [13, 32] employed graph neural networks for this task, capitalizing on the natural graph structure of molecules. However, most of these methods tend to directly apply existing frameworks from other domains or perform independent feature extraction for each component of the reaction followed by a simple aggregation, potentially overlooking the rich information in complex chemical reactions.

Beyond the insufficient utilization of reaction information, current methods simply regard reagents as a component of reactants for encoding when integrating reaction conditions into the reaction representation. However, this approach does not allow the model to consider any non-molecular reaction conditions, including temperature and other environmental factors [11]. Furthermore, this narrow focus also impedes the applicability of current methods to datasets that provide experimental operations (e.g., stir and filter) in the form of natural language [22]. Hence, we aim to develop a chemical reaction representation learning model that integrates a richer set of chemical information and is adaptable to various modalities of reaction conditions.

To address the aforementioned shortcomings, we proposed RAlign, a powerful chemical reaction representation learning model for multiple downstream tasks. Reaction centers and the reaction process play pivotal roles in determining the outcome of the reaction [44]. Drawing inspiration from the imaginary transition structures of organic reactions [9], we incorporate information fusion operations for corresponding atom pairs in reactants and products within our encoder. This approach explicitly models the chemical bond changes during reactions. Furthermore, we have proposed a reaction-center-aware decoder to assist the model in focusing on key functional groups. To accommodate various modalities of reaction conditions, we have employed an adapter structure to integrate these conditions into the chemical reaction representations. We have evaluated our model on a range of tasks, including reaction condition prediction, reaction yield prediction, and reaction selectivity prediction. Our model has achieved remarkable performance across all tasks, even surpassing the baselines with extensive pretraining. **The contribution of this work can be summarized as:**

- To the best of our knowledge, this work is the first to model atomic correspondence between reactants and products in the extraction of reaction representations, and it is also the first to design a graph backbone specifically for chemical reaction representation learning.
- We propose a reaction condition integration mechanism that enables the model to assimilate various chemical reaction conditions and leverages previous work to enhance the chemical reaction representations.

- Extensive experiments demonstrate that our model has achieved remarkable success in a variety of tasks related to chemical reactions. Particularly, our model has demonstrated a 25% increase in top-1 accuracy for reaction condition prediction task on the USPTO_CONDITION dataset, surpassing the strongest baseline.

2 Related Work

2.1 Molecular Representation Learning

Existing methods for molecule representation learning are categorized into SMILES-based and structure-based approaches. SMILES [52], as a textual representation, allows for molecule encoding with language models [17], but it may overlook molecular topological information. Thus, there's a growing interest in structure-based methods, which are further divided into fingerprint-based and graph neural network (GNN)-based approaches. Fingerprint-based methods, originating from the Morgan fingerprint [34], face limitations due to their manual crafting and lack of end-to-end training [19], especially with complex structures and large datasets. Conversely, GNN-based learning [18, 20, 21, 54, 57] has gained popularity for its effectiveness.

Chemical reaction representation learning, crucial for industrial applications, e.g., reactivity prediction and reaction condition optimization, has seen less focus compared to molecular representation. Current chemical reaction representation learning approaches [31, 44] often be implemented by simple concatenation of molecular representation, or rely on the straightforward application of existing backbones without domain knowledge integration. This study presents a novel model that captures molecular differences before and after reactions and incorporates reaction center information, enhancing the robustness of chemical reaction representations.

2.2 Reaction Condition Prediction

The chemical reaction condition prediction task aims to identify suitable catalysts, solvents, reagents, or other conditions for a given chemical reaction involving specific reactants and products. Existing methods can be broadly categorized into two types. The first category transforms the problem into a classification task within a predefined condition pool. GCNN [32] employs graph neural networks for multi-label classification to predict the presence of each molecule in the reaction condition combination. FPRCR [10] and Parrot [51], focusing on reaction condition combinations with fixed compositional elements, utilize fingerprinting and BERT [7] respectively, to predict the specific reagents for each component. The second category is not constrained by a predefined reagent library. These methods [2, 31] leverage language models to generate SMILES strings of the chemical reagents as reaction conditions. However, these approaches depend on manual feature selection based on expert knowledge and do not offer a generalizable prediction model with robust reaction representation capabilities.

2.3 Reaction Yield Prediction & Reaction Selectivity Prediction

Reaction yield and selectivity prediction are fundamentally similar tasks, both requiring regression of a numerical value given a chemical reaction and its conditions. Consequently, many methods are applicable to both problems. Existing strategies can be divided into two primary categories: fingerprint-based and deep-learning-based. Fingerprint-based approaches construct chemical reaction representations on the basis of hand-crafted molecular fingerprints through various combinatorial strategies. DRFP [38] has designed a fingerprint that reflects the differences between reactants and products, serving as a chemical reaction representation. MFF [41] leverages a variety of fingerprints to enhance model performance.

Deep-learning methods predominantly employ large-scale pre-trained models to extract chemical reaction representations [13, 31, 44, 45, 47], aiming for enhanced generalizability. The reaction yield prediction task often grapples with noisy data, leading some studies [4, 26] to address this by adjusting the training loss to incorporate uncertainty, thus refining model performance. In addressing reaction selectivity prediction, there is a preference for incorporating quantum chemical information. For example, the works of Li et al., Li et al. and Zahrt et al. have incorporated descriptors such as average steric occupancy and electronic properties predicated on structures optimized via DFT calculations. Guan et al. designed a GNN that depends on the lowest-lying conformer calculated by DFT. However, the computation of these quantum chemical descriptors is exceedingly time-intensive, potentially necessitating several days for a modest sample size, which poses a challenge for its application to large-scale datasets. Furthermore, many deep-learning methods continue to directly apply backbone architectures from other domains. There is a clear demand for a backbone that can seamlessly integrate chemical information to extract potent chemical reaction representations, which remains an area for worthy exploration.

3 Preliminary

3.1 Reaction Condition Combination Generation/Prediction

In this paper, the term “reaction condition combinations” specifically refers to the combination of catalysts, solvents, and other chemical reagents. The distinction between the prediction task and the generation task lies in the fact that the prediction task utilizes a pre-defined library of chemical reagents from which appropriate combinations are selected; in contrast, the generation task does not require a pre-defined library, and the model must generate suitable molecular combinations of reagents *de novo*.

3.2 Reaction Selectivity Prediction

The same set of reactants can yield different products under varying conditions. The task of reaction selectivity prediction aims to forecast the proportions of different products that can be generated from a given set of reactants under specified conditions. Reaction selectivity usually includes regio-selectivity and chiral-selectivity. The former refers to the production of different products due to differences in reaction sites, while the latter refers to the production of a pair of mirror-symmetrical products. The tendency to produce

a certain product is related to the corresponding intermediate state energy, which is termed ΔG^\ddagger . Previous work [46] about transition state theory indicates that there is an exponential relationship between ΔG^\ddagger and chemical reaction rate, which means that the lower the energy of the intermediate state, the higher the reaction rate, and the more inclined to form the corresponding product. To be specific [36], the reaction ratio of producing product *A* and *B* could be formulated as:

$$\frac{r_A}{r_B} = \exp \frac{\Delta \Delta G^\ddagger}{RT} \quad (1)$$

where *R* is gas constant, *T* is the Kelvin temperature, and $\Delta \Delta G^\ddagger$ represents the differences in ΔG^\ddagger between different reaction pathways for product *A* and *B*. In most cases, people use the ratio of product *A* and *B*, i.e. $\frac{r_A}{r_B}$, to approximate the selectivity of chemical reactions. Then the reaction selectivity prediction, which might involve multiple reactions and products, can be simplified into the prediction of ΔG^\ddagger of one chemical reaction with a single product.

3.3 Notations about Chemical Reactions

In the realm of chemical reactions, the fundamental components are the reactants and products. These can be represented as two distinct molecular graphs, denoted by $G_R = (V_R, E_R)$ and $G_P = (V_P, E_P)$ respectively. Here, V_P and V_R symbolize the set of atoms, while E_P and E_R represent the chemical bonds that interconnect them.

A cardinal principle in chemical reactions is the conservation of atoms. This principle dictates that for every atom present in the products, there exists a unique corresponding atom in the reactants. Let $V_R = \{v_1^R, v_2^R, \dots, v_n^R\}$ and $V_P = \{v_1^P, v_2^P, \dots, v_m^P\}$ with $n \geq m$. For the sake of clarity and consistency in subsequent discussions, we stipulate that for all $1 \leq i \leq m$, atom v_i^R is the unique counterpart to the atom v_i^P in the products. And we define the atoms of reactants do not appear in the products as leaving group, denoted as $V_L = \{v_{m+1}^R, v_{m+2}^R, \dots, v_n^R\}$.

We further denote the set of reaction centers as V_{rc} , which is a subset of all the atoms from both reactants and products. An atom is considered as a reaction center as long as it meets one of the following criteria:

- It is an atom from either the reactants or products that is the terminus of a chemical bond undergoing alteration during the reaction.
- It is an atom from the reactants (or products) whose hydrogen count is discordant with that of its corresponding atom in products (or reactants).
- It is an atom that is a one-hop neighbor of an atom satisfying the first two conditions.
- It is a part of the leaving group.

4 Methodology

We introduce a novel chemical reaction feature extractor named RAlign with an encoder-decoder architecture, as illustrated in Fig. 1. The encoder incorporates the atomic correspondence between reactants and products to generate robust features for the chemical reaction. The decoder then integrates the output features from the encoder according to the reaction center information to produce different formatted outputs tailored to downstream tasks.

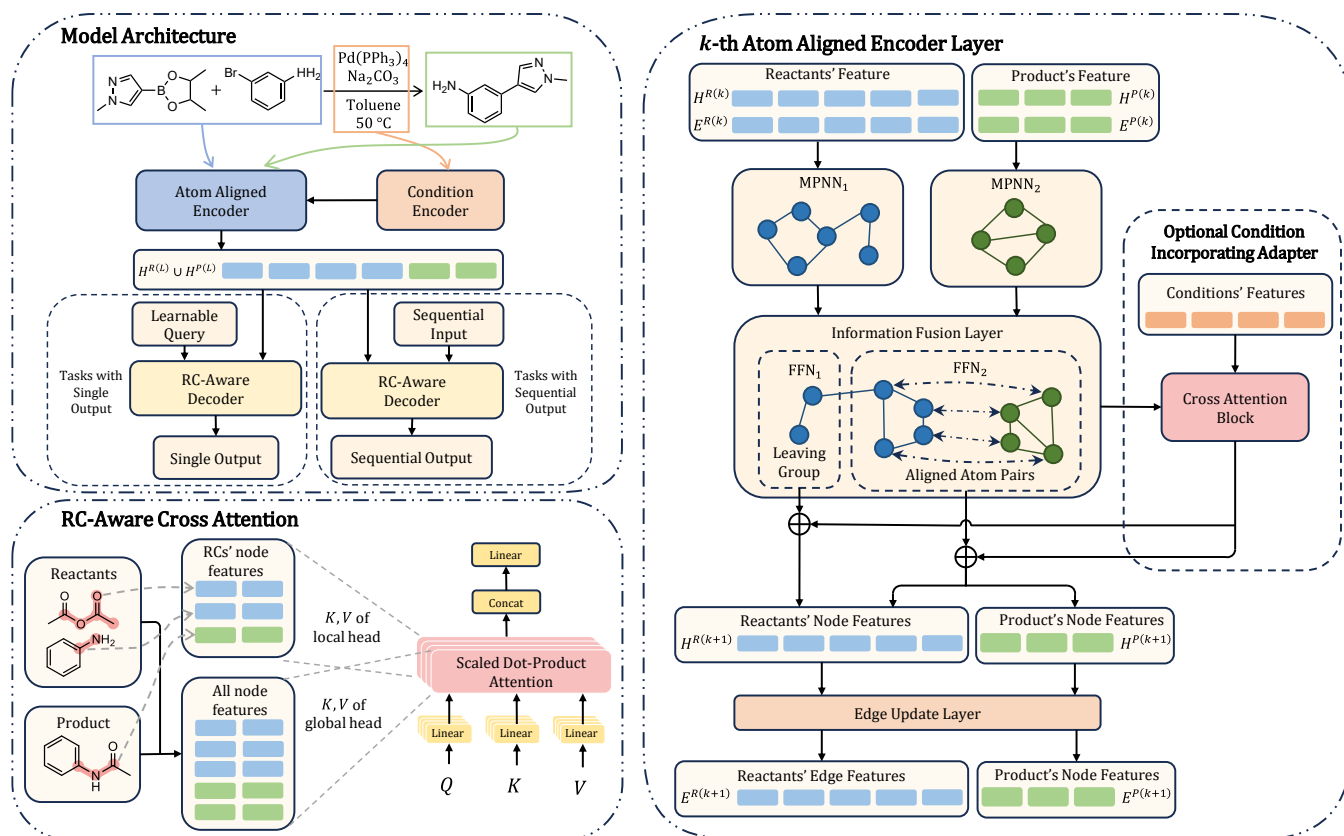


Figure 1: Overview of RAlign. For a given chemical reaction, the molecule graphs of reactants and products, along with their atomic correspondence, are input into a L -layer Atom Aligned Encoder to extract reaction node features $H^{P(L)}$ and $H^{R(L)}$. If the reaction conditions are also provided, they are encoded by a condition encoder and merged into $H^{P(L)}$ and $H^{R(L)}$ via an adapter structure proposed in this study. The resulting features are then processed by the RC-aware decoder to produce outputs for subsequent tasks. We have tailored two decoders for both sequential output and single output, both featuring an RC-aware cross-attention layer to concentrate on key reaction motifs.

4.1 Atom Aligned Encoder

Understanding chemical reaction mechanisms is fundamental to developing robust representations in cheminformatics. Despite significant advancements, our grasp of these mechanisms remains incomplete, and the annotation of reaction mechanisms necessitates considerable effort from chemical experts. To navigate this challenge, we have adopted a pragmatic approach. At present, there are well-established tools [5, 42] that can delineate the atomic correspondence between reactants and products in chemical reactions. Integrating this atomic mapping information into models can enhance the identification of similarities and differences between reactants and products, thereby improving the model’s capacity to understand the evolution of chemical reactions. Driven by these considerations, we introduce the Atom Aligned Encoder, a model engineered to assimilate both the chemical reaction and its associated atom-mapping data for effective encoding of chemical reactions.

The Atom Aligned Encoder is structured as a series of identical blocks that iteratively refine the node and edge features, mirroring the iterative process of GNNs. Within each block, we deploy

two distinct message-passing neural network (MPNN) layers for reactants and products, respectively. These layers amalgamate both node and edge features in accordance with the molecular structures, yielding intermediate node features. Subsequently, an information fusion layer is implemented to integrate intermediate features of corresponding atom pairs between reactants and products. Additionally, the intermediate node features of atoms that are absent in the products are further refined through an auxiliary feed-forward network. Ultimately, the edge features are updated contingent upon the node features of the edge termini.

Given a chemical reaction with reactants $R = (V_R, E_R)$ and products $P = (V_P, E_P)$, where $V_R = \{v_1^R, v_2^R, \dots, v_n^R\}$ and $V_P = \{v_1^P, v_2^P, \dots, v_m^P\}$, we denote the output node feature of k -th block for v_i^R (resp. v_i^P) as $h_i^{R(k)}$ (resp. $h_i^{P(k)}$) and the output edge feature of the k -th block for $(v_i^R, v_j^R) \in E_R$ (resp. $(v_i^P, v_j^P) \in E_P$) as $e_{i,j}^{R(k)}$ (resp. $e_{i,j}^{P(k)}$). We further delineate the collection of the output node features and edge features for both reactants and products of the

k -th block, as articulated in Eq. 2.

$$\begin{aligned} H^{R(k)} &= \{h_1^{R(k)}, h_2^{R(k)}, \dots, h_n^{R(k)}\}, \\ H^{P(k)} &= \{h_1^{P(k)}, h_2^{P(k)}, \dots, h_m^{P(k)}\}, \\ E^{R(k)} &= \{e_{i,j}^{R(k)} \mid (v_i^R, v_j^R) \in E_R\}, \\ E^{P(k)} &= \{e_{i,j}^{P(k)} \mid (v_i^P, v_j^P) \in E_P\}. \end{aligned} \quad (2)$$

Then the k -th block of Atom Aligned Encoder can be mathematically summarized as

$$\begin{aligned} \{\tilde{h}_i^{R(k)}, \tilde{h}_i^{R(k)}, \dots, \tilde{h}_i^{R(k)}\} &= \text{MPNN}_1 \left(H^{R(k-1)}, E^{R(k-1)} \right), \\ \{\tilde{h}_i^{P(k)}, \tilde{h}_i^{P(k)}, \dots, \tilde{h}_i^{P(k)}\} &= \text{MPNN}_2 \left(H^{P(k-1)}, E^{P(k-1)} \right), \\ \left[\tilde{h}_i^{R(k)} \parallel \tilde{h}_i^{P(k)} \right] &= \text{FFN}_1 \left(\left[\tilde{h}_i^{R(k)} \parallel \tilde{h}_i^{P(k)} \right] \right), 1 \leq i \leq m, \\ h_i^{R(k)} &= \text{FFN}_2 \left(\tilde{h}_i^{R(k)} \right), m < i \leq n, \\ e_{i,j}^{R(k)} &= \text{FFN}_3 \left(\left[h_i^{R(k)} \parallel h_j^{R(k)} \right] \right), \\ e_{i,j}^{P(k)} &= \text{FFN}_4 \left(\left[h_i^{P(k)} \parallel h_j^{P(k)} \right] \right), \end{aligned} \quad (3)$$

where $[\cdot \parallel \cdot]$ represents the concatenation of features, $H^{R(0)}$, $H^{P(0)}$, $E^{R(0)}$ and $E^{P(0)}$ represent the initial node and edge features for reactants and products. In Eq. 3, $\tilde{h}_i^{R(k)}$ (*resp.* $\tilde{h}_i^{P(k)}$) represents the intermediate features of the k -th block for v_i^R (*resp.* v_i^P). Residual connections and layer normalization [3] are implemented across different layers to expedite model convergence and facilitate the stabilization of the training process. The detail implementation of initial feature extraction and the message passing network is presented in Appendix B.

4.2 Incorporating Reaction Conditions

The formatting of chemical reaction conditions varies across different datasets, contingent upon the specific application scenarios. Moreover, the conditions of chemical reactions might incorporate multimodal information. For example, the Reaxys dataset [51] details reaction conditions by specifying supplementary reagents and precise temperatures. Conversely, in the research conducted by Yoshikawa et al. [55], these conditions are translated into a uniform series of experimental protocols. Furthermore, in predictive tasks such as forecasting reaction conditions, reaction conditions will not be provided as input. This underscores the necessity for a modular design in the chemical reaction condition incorporation module, one that can be easily interchanged or omitted, rather than being a rigid component of the encoder architecture. Consequently, we propose a versatile mechanism for integrating chemical reaction conditions, ensuring its adaptability to a range of applications within the field of cheminformatics.

Drawing inspiration from multimodal conditional image generation works such as T2IAdapter [35] or ControlNet [58], which adeptly integrate multimodal information and effectively leverage prior research to enhance model performance, we have chosen to implement an adapter structure for incorporating reaction conditions. This approach allows us to seamlessly assimilate these conditions without necessitating modifications to the underlying

architecture of the Atom Aligned Encoder. Let us assume that the reaction condition for a given reaction has been encoded into a feature matrix $C \in \mathbb{R}^{c \times d}$, where c denotes the number of features and d signifies the dimension of each feature. For each block within the Atom Aligned Encoder, we utilize multi-head attention to integrate the reaction condition information into its output node features. Subsequently, we employ these node features, now imbued with reaction condition information, to generate the output edge features. Mathematically, with the incorporation of chemical reaction conditions, the output node features and edge features of the k -th block in Atom Aligned Encoder is modified as follows:

$$\begin{aligned} \left[\tilde{h}_i^{R(k)} \parallel \tilde{h}_i^{P(k)} \right] &= \text{FFN}_1 \left(\left[\tilde{h}_i^{R(k)} \parallel \tilde{h}_i^{P(k)} \right] \right), 1 \leq i \leq m, \\ \tilde{h}_i^{R(k)} &= \text{FFN}_2 \left(\tilde{h}_i^{R(k)} \right), m < i \leq n, \\ h_i^{R(k)} &= \tilde{h}_i^{R(k)} + \text{Attn}_1 \left(\tilde{h}_i^{R(k)}, C, C \right), \\ h_i^{P(k)} &= \tilde{h}_i^{P(k)} + \text{Attn}_2 \left(\tilde{h}_i^{P(k)}, C, C \right), \\ e_{i,j}^{R(k)} &= \text{FFN}_3 \left(\left[h_i^{R(k)} \parallel h_j^{R(k)} \right] \right), \\ e_{i,j}^{P(k)} &= \text{FFN}_4 \left(\left[h_i^{P(k)} \parallel h_j^{P(k)} \right] \right), \end{aligned} \quad (4)$$

where the intermediate node features $\tilde{h}_i^{R(k)}$ and $\tilde{h}_i^{P(k)}$, as described in Eq. 3, are the outputs of the MPNN layer. $\text{Attn}(Q, K, V)$ in Eq. 4 denotes the vanilla multihead attention [48], which can be mathematically expressed as

$$\begin{aligned} o_i &= \text{softmax} \left(\frac{QW_i^Q(KW_i^K)^T}{\sqrt{d}} \right) VW_i^V, \\ \text{Attn}(Q, K, V) &= [o_1 \parallel o_2 \parallel \dots \parallel o_h] W^O \end{aligned} \quad (5)$$

where W_i^Q , W_i^K , W_i^V and W^O are learnable parameters, $[\cdot \parallel \cdot]$ represents the concatenation of features, h is the number of heads and d is the dimension of the key vectors.

4.3 Reaction-Center-Aware Decoders

The decoder takes the encoded node features $H^{R(L)}$ and $H^{P(L)}$ from Atom-Aligned Encoder with L blocks as input and generates outputs in various formats depending on the task at hand. In this section, we introduce decoder architectures tailored for both sequential generation tasks and tasks with a single output. Given that reaction centers record the key functional groups involved in chemical reactions and play a decisive role in their properties [23], we have designed a Reaction-Center-Aware Decoder that explicitly integrates information about reaction centers into the chemical reaction representations applied to downstream tasks.

We first introduce the Reaction-Center-Aware (RC-aware) cross-attention mechanism, which is adapted from the local-global decoder of the Retroformer [50]. The RC-aware cross-attention is a specialized attention mechanism where half of the attention heads function identically to the standard attention, while the other half is restricted to accessing only the node features of the reaction centers V_{rc} . The formulation for attention heads i within the RC-aware cross-attention mechanism, which are constrained to accessing

only the reaction centers, is articulated as follows:

$$\begin{aligned}\alpha_l^1 &= \frac{\exp(k_l^R q^T)}{\sum_{v_j^R \in V_{rc}} \exp(k_j^R q^T) + \sum_{v_j^P \in V_{rc}} \exp(k_j^P q^T)}, \\ \alpha_l^2 &= \frac{\exp(k_l^P q^T)}{\sum_{v_j^R \in V_{rc}} \exp(k_j^R q^T) + \sum_{v_j^P \in V_{rc}} \exp(k_j^P q^T)}, \\ o_i &= \sum_{v_i^R \in V_{rc}} \frac{\alpha_l^1}{\sqrt{d}} h_l^{R(L)} W_i^V + \sum_{v_i^P \in V_{rc}} \frac{\alpha_l^2}{\sqrt{d}} h_l^{P(L)} W_i^V, \\ [k_l^R, k_l^P, q] &= [h_l^{R(L)} W_i^K, h_l^{P(L)} W_i^K, Q W_i^Q],\end{aligned}\quad (6)$$

where W_i^Q , W_i^K , W_i^V are learnable parameters, Q is the query vector and d is the dimensionality of the key vectors. The output of RC-aware cross-attention is summarized as

$$\text{RCAttn}(Q, H^{R(L)} \cup H^{P(L)}, V_{rc}) = [o_1 \| o_2 \| \dots \| o_h] W^O, \quad (7)$$

where W^O is learnable parameter, $[\cdot \| \cdot]$ represents the concatenation of features and h is the number of heads.

Then for sequential generation tasks, we replace the cross-attention layers of vanilla transformer decoder [48] with the RC-aware cross-attention, thereby customizing our decoder. In the case of tasks that require a numerical output, such as chemical reaction yield prediction, we utilize a learnable query vector within the RC-aware cross-attention mechanism to derive a reaction-level representation. Subsequently, this representation is fed into a feed-forward network to generate the final output.

5 Experiments

To demonstrate the capability of our model to extract potent reaction embeddings and apply them to a variety of downstream tasks, we conducted extensive experiments, including predictions of reaction condition combinations, reaction yield, and reaction selectivity. For ease of understanding, we have depicted the pipelines for different tasks in Fig 2.

5.1 Reaction Condition Combination Prediction/Generation

Dataset. We use USPTO_CONDITION dataset to evaluate performance of our model on reaction condition combination prediction task. This dataset comprises 680,741 reactions, with each reaction condition being consistently composed of one catalyst, two reagents, and two solvents. We have directly utilized the pre-processed data from Wang et al. and further employed RXNMapper [42] to augment the chemical reactions with atom mapping. For reaction condition generation tasks, we use USPTO_500MT dataset for evaluation. We generate and sort the reagents according to a certain rule, whose detail is displayed in Appendix C.2. The tokenization on the SMILES representations of the reagents is aligned with the work [43].

Metric. In this section, we assess the predictive performance for the whole reaction condition combinations as well as for each constituent element within the reaction conditions. We use the conventional top- k accuracy to evaluate the performance of model. A prediction is considered as correct if and only if all the molecules of it are correctly predicted. The order of the constituents is not

one of the criteria for determining whether a prediction is correct. When a reaction in the test set has multiple recorded reaction combinations, a prediction is considered correct if it is completely consistent with any one of them.

Baselines. We compare our method against four baselines for reaction condition prediction tasks. GCNN [32] uses message-passing networks to extract reaction representation and then predicts the reaction condition combinations. FPCR [10] utilizes the fingerprints of reactants, products, and the components of the reaction conditions that have already been predicted as inputs to predict the next composition of reaction condition combinations. Parrot-LM-E [51] and Reagent Transformer [2] are two transformer-based models that have been developed, respectively, based on the checkpoint of BERT [7] for Parrot-LM-E and the checkpoint of the Molecular Transformer [43] for Reagent Transformer. Note that the Parrot-LM-E and FPCR are specifically designed for reaction condition combinations with a fixed number of components, so they have not been applied to the USPTO_500MT dataset. We also report the experimental results of T5chem [31], a text-to-text transformer model, on the USPTO_500MT dataset. The results from a model that was finetuned from a checkpoint pretrained on a large-scale reaction dataset, as well as the results from a model trained from scratch, have both been reported by us.

Performance Evaluation. The USPTO_CONDITION dataset’s result is summarized in Table 2 and Table 1. And the results of USPTO_500MT is summarized in Table 3. From the table we can find that on USPTO_CONDITION dataset, our model achieves a top-1 accuracy of 34.30%, a top-5 accuracy of 52.82% and a top-10 accuracy of 59.22%, surpassing the strongest baseline Parrot-LM_E by 6.88%, 5.84% and 8.27% respectively. When evaluating the prediction accuracy for each type of component within reaction conditions, it is observed that our model significantly outperforms all the baseline models across all metrics. Particularly in the prediction of solvents, our model attains a top-1 accuracy of 50.45% and a top-10 accuracy of 79.18%, surpassing the strongest baseline by 6.25% and 13.02%, respectively. On USPTO_500MT dataset, our model achieves a top-1 overall accuracy of 26.84% and an top-10 overall accuracy of 50.25%, which exceeds the strongest baseline that did not utilize pretraining by 7.64% and 11.55%. Additionally, it can be observed that our model exhibits performance almost equivalent to that of the T5Chem model trained on a large-scale reaction dataset. The aforementioned performance indicates that our model is capable of extracting robust reaction representations for both predictive and generative tasks.

5.2 Reaction Yield Prediction

Dataset. We use Buchwald-Hartwig dataset [1] to evaluate the performance of our model on reaction yield prediction task. The dataset provides 10 random splits and four ligand-based out-of-sample splits for evaluation. The test sets under the four out-of-sample data split contain reaction additives which are not included in the train sets. We use the raw data and data split provided by Probst et al. and add the atom mapping for reactions according to the reaction template. In this study, we have standardized the yields to a range of 0 to 100. The statistical information of different splits is summarized in Appendix A.

Table 1: Accuracy of each component on USPTO_CONDITION dataset for reaction condition prediction. The detailed prediction accuracy on each type of components is displayed. The best performance is in bold and the second-best is underlined.

Method	Top- <i>k</i> accuracy (%)											
	catalyst				solvents				reagents			
	1	3	5	10	1	3	5	10	1	3	5	10
Parrot-LM_E [51]	<u>92.12</u>	<u>94.91</u>	<u>95.97</u>	<u>97.28</u>	<u>44.20</u>	<u>59.23</u>	<u>63.71</u>	<u>66.16</u>	<u>46.47</u>	<u>62.04</u>	<u>68.19</u>	<u>73.93</u>
GCNN [32]	90.59	91.80	92.40	93.39	32.39	46.02	52.51	61.06	35.84	46.37	50.61	55.99
Reagent Transformer [2]	89.80	93.30	94.52	95.88	37.97	51.29	57.47	65.44	39.11	55.20	61.83	69.80
FPRCR [10]	91.22	92.82	93.57	94.74	38.51	49.72	54.64	61.56	37.54	47.95	52.69	58.48
Ours	92.98	95.75	96.60	97.52	50.45	66.81	72.75	79.18	49.68	63.46	68.69	75.21

Table 2: Overall accuracy of reaction condition prediction on USPTO_CONDITION dataset. The best performance is in bold. The second-best performance is underlined.

Model	Top- <i>k</i> accuracy (%)			
	1	3	5	10
GCNN [32]	12.81	21.95	26.40	32.17
FPRCR [10]	16.90	26.38	31.16	36.96
Reagent Transformer [2]	22.74	34.09	39.36	46.01
Parrot-LM-E [51]	<u>27.42</u>	<u>41.86</u>	<u>46.98</u>	<u>50.95</u>
Ours	34.30	47.60	52.82	59.22

Table 3: Overall accuracy of reaction condition generation on USPTO_500MT dataset. The best performance is in bold. The second-best performance is underlined.

Model	Top- <i>k</i> accuracy (%)			
	1	3	5	10
T5Chem-pretrained [31]	<u>26.2</u>	<u>39.4</u>	45.0	51.6
GCNN [32]	4.92	12.66	18.35	25.19
Reagent Transformer [2]	19.20	27.24	30.81	35.20
T5Chem-from-scratch [31]	17.50	28.00	32.8	38.70
Ours	26.84	39.58	<u>44.61</u>	<u>50.25</u>

Table 4: The results on Buchwald-Hartwig dataset under four out-of-sample split. The best performance is in bold. The second-best performance is underlined.

Model	Test1			Test2			Test3			Test4		
	MAE ↓	RMSE ↓	R ² ↑	MAE ↓	RMSE ↓	R ² ↑	MAE ↓	RMSE ↓	R ² ↑	MAE ↓	RMSE ↓	R ² ↑
DRFP [38]	7.9492	11.3285	0.8273	9.0878	13.5990	0.7480	10.0901	15.8577	0.6814	<u>12.7572</u>	<u>19.1300</u>	0.4769
Chemprop [14]	8.5883	12.3130	0.7960	10.5984	14.2913	0.7217	10.4930	15.4690	0.6969	14.5839	20.4564	0.4018
YieldBert [45]	7.5416	<u>11.2156</u>	0.8308	7.4349	10.8098	0.8408	9.6488	15.2584	0.7051	13.5600	19.3862	0.4627
T5Chem [31]	<u>7.1283</u>	11.2242	<u>0.8385</u>	<u>6.7693</u>	<u>10.4041</u>	<u>0.8801</u>	<u>9.0982</u>	<u>14.3431</u>	<u>0.7665</u>	13.4069	19.7521	0.6051
Ours	5.4643	8.6916	0.8983	5.4182	8.0480	0.9117	8.6299	12.4570	0.8034	12.0324	18.0998	<u>0.5317</u>

Table 5: The results on Buchwald-Hartwig dataset under ten random splits. The best performance is in bold. The second-best performance is underlined.

Model	MAE ↓	RMSE ↓	R ² ↑
DRFP [38]	4.0995 ± 0.1191	6.2424 ± 0.2636	0.9474 ± 0.0050
Chemprop [14]	4.6430 ± 0.1405	6.4306 ± 0.1938	0.9441 ± 0.0042
YieldBert [45]	<u>3.5532 ± 0.1600</u>	<u>5.4480 ± 0.3240</u>	<u>0.9599 ± 0.0050</u>
T5Chem [31]	3.5059 ± 0.1562	5.3181 ± 0.2482	0.9662 ± 0.0034
Ours	3.6331 ± 0.1259	5.5649 ± 0.2839	0.9581 ± 0.0049

Baselines. We use four powerful baselines for comparison. The first is DRFP [38], a kind of chemical reaction fingerprint for yield prediction. The second is Chemprop [14], a kind of Message Passing Network encoding multi-molecules or reactions. The third is YieldBert [45], a transformer pretrained on Pistachio dataset [33] using self-supervised tasks. And the fourth is T5Chem [31], a language

model pretrained on PubMed dataset [24] with a self-supervised task and USPTO_500MT dataset [31] with five different supervised tasks including reaction yield prediction.

Implementation Details. It should be noted that the number of distinct reagents in the reaction conditions of Buchwald-Hartwig dataset is less than 50, which makes it challenging to train a reaction condition encoder from scratch. Thus we use a lightweight pre-trained molecular encoder [16] as our reaction condition encoder. For detailed information, please refer to Appendix B.4.

Performance Evaluation. The average results of ten random splits of Buchwald-Hartwig dataset is summarized in Table 5 and the results of four out-of-sample splits are summarized in Table 4. Table 5 indicates that our model has achieved an average R² of 0.958 and an average MAE of 3.633 under ten random splits, placing it in the third position among all the compared methods. However, it is important to note that our model, which has not been pretrained on large-scale reaction data, is not significantly outperformed by two deep learning models that have. The difference in R² between

Table 6: The results on C-H functionalization selectivity dataset under random splits. The best performance is in bold. The second-best performance is underlined.

Model	MAE ↓	RMSE ↓	R^2 ↑
MFF [41]	2.2923 ± 0.0400	2.9388 ± 0.0393	0.5891 ± 0.0095
DRFP [38]	0.9435 ± 0.0293	1.2943 ± 0.0387	0.9203 ± 0.0042
Chemprop [14]	<u>0.3593 ± 0.0099</u>	0.5396 ± 0.0299	0.9861 ± 0.0015
RXNFP [44]	0.3744 ± 0.0094	<u>0.5378 ± 0.0204</u>	<u>0.9862 ± 0.0010</u>
T5Chem [31]	0.6272 ± 0.0184	0.8213 ± 0.0226	0.9822 ± 0.0011
Ours	0.3267 ± 0.0159	0.5110 ± 0.0292	0.9875 ± 0.0014

Table 7: The results on thiol addition selectivity dataset under random splits. The best performance is in bold. The second-best performance is underlined.

Model	MAE ↓	RMSE ↓	R^2 ↑
MFF [41]	0.1421 ± 0.0093	<u>0.2122 ± 0.0169</u>	0.9055 ± 0.0119
DRFP [38]	<u>0.1481 ± 0.0094</u>	0.2120 ± 0.0147	<u>0.9056 ± 0.0117</u>
Chemprop [14]	0.1626 ± 0.0118	0.2283 ± 0.0174	0.8907 ± 0.0130
RXNFP [44]	0.1650 ± 0.0111	0.2313 ± 0.0197	0.8872 ± 0.0193
T5Chem [31]	0.1662 ± 0.0108	0.2417 ± 0.0182	0.8920 ± 0.0121
Ours	0.1535 ± 0.0085	0.2202 ± 0.0118	0.8982 ± 0.0103

our model and the strongest baseline is less than 0.01, and the gap in terms of MAE is less than 0.1. In the out-of-sample settings, our model demonstrates superior performance under various evaluation metrics. For instance, it attains an R^2 score of 0.898, surpassing the strongest baseline by 0.060. Notably, our model outperforms other baselines in all metrics, excluding the R^2 metric in the Test4 data split, by a significant margin. Furthermore, our model records an approximate 2.000 improvement in RMSE across all data splits.

The aforementioned experimental results demonstrate that our model can extract powerful reaction representations even without the aid of pretraining based on large-scale chemical reaction data. Additionally, the results from the out-of-sample datasets confirm the advantages of our adapter design as mentioned in Sec. 4.2, which allows our model to conveniently leverage the previous works to enhance performance, even if such works were not specifically designed for reaction encoding.

5.3 Reaction Selectivity Prediction

Datasets. We use the C-H functionalization dataset [30] created by Li et al. to demonstrate the regio-selectivity prediction performance, and use the experimental dataset [29, 56] regarding chiral phosphoric acid-catalyzed thiol addition to N-acylimines created by Zahrt et al. to illustrate the enantioselectivity predictive performance. There are 6114 chemical reactions in C-H functionalization Dataset, and thiol addition Dataset contains 43 catalysts and 5×5 reactants combination, which form 1075 reactions. These datasets was randomly divided into a training set and a test set with a ratio of 7:3 for 10 times.

Baseline. Considering that the reaction selectivity prediction task is fundamentally a regression problem, we have adapted three deep-learning models originally designed for reaction yield prediction, Chemprop [14], T5chem [31] and RXNFP [44], to this task.

Additionally, two fingerprint-based methods are compared as well. In detail, DRFP [38] calculate the fingerprint of the symmetric difference between the n-grams of reactants and products, while MFF [41] leverages multiple fingerprint features of all the molecules in one reaction as input of the regressor.

Performance Evaluation. The results on two datasets are summarized in Table 6 and Table 7. On C-H functionalization Dataset, our model achieves the best performance among all the compared methods across all metrics, with an average MAE of 0.327, an average RMSE of 0.511, and an average R^2 of 0.988. Notably, our models outperforms two baselines RXNFP and T5chem, which are pre-trained on large-scale reaction dataset. These results demonstrate that our model exhibits architectural superiority and a stronger understanding of chemical reactions compared to existing methods.

On the thiol addition dataset, two fingerprint-based methods achieve the best results. Our model ranks third with an average MAE of 0.154, an average RMSE of 0.220, and an average R^2 of 0.898. Deep-learning-based models do not stand out in this dataset, which is attributed to the dataset’s sparsity, consisting of only 10 different reactants and 43 different catalysts. This sparsity is insufficient to support model training. However, it is noteworthy that our model still outperforms all other deep-learning methods, including two pretrained models, even without the aid of reaction data pretraining, showcasing the superiority of our model architecture.

Furthermore, when dealing with extremely small-scale datasets, the performance of our model can be further enhanced by incorporating more rule-based features, such as the electronic distribution of atoms, as our model does not impose restrictions on the implementation of the MPNN network used to encode reactants and products. Large-scale pretraining on a reaction dataset will also be beneficial. However, these improvement methods are beyond the scope of this paper, and we will reserve them for future work.

5.4 Ablation Study

We investigate the effects of different components in our proposed pipelines. We remove or substitute the distinct components of our model and subject them to testing on the USPTO_500MT dataset and the random split setting of the Buchwald-Hartwig Dataset. The result is summarized in Table 8.

Atom Aligned Encoder. We remove the information fusion layers of Atom Aligned Encoder. Under this circumstance, the Atom Aligned Encoder has been simplified into a network composed of two separate MPNN networks that encode reactants and products, respectively. As observed in Table 8, the removal of the information fusion layer has led to a decrease in the model’s performance across all metrics for different tasks, especially in terms of the top-1 and top-3 accuracy for reaction condition prediction on the USPTO_500MT dataset. This suggests that by incorporating the alignment of atoms before and after the reaction into the model, the Atom Aligned Encoder can more effectively discern the differences between the molecules before and after the reaction, thus offering more robust reaction representations for downstream tasks.

Reaction-Center-Aware Decoders. We replace the RC-aware cross-attention layers with the original cross-attention layer proposed in [48]. Table 8 demonstrates a decline in model performance in terms of all metrics for both the sequential generation tasks and

Table 8: Effects of different modules on USPTO_500MT Dataset for reaction condition prediction task and on the random split setting of Buchwald-Hartwig dataset for reaction yield prediction task. The best performance is in bold.

Model	USPTO_500MT				Buchwald-Hartwig		
	Top- <i>k</i> Accuracy(%)				MAE ↓	RMSE ↓	R^2 ↑
	1	3	5	10			
Full Version	26.84	39.58	44.61	50.25	3.6331 ± 0.1259	5.5649 ± 0.2839	0.9581 ± 0.0049
- Atom Aligned Encoder	26.01	38.79	43.99	50.19	3.7289 ± 0.1291	5.7318 ± 0.2520	0.9556 ± 0.0044
- Reaction-Center-Aware Decoders	26.29	39.14	43.91	49.82	3.6967 ± 0.1710	5.7845 ± 0.3948	0.9547 ± 0.0066

the task that requires a reaction-level representation. This clearly demonstrates that the RC-aware cross-attention mechanism enables the model to focus on the core functional groups of the reaction and comprehend the reaction process, thereby leading to performance improvements.

6 Conclusion

In this paper, we propose RAlign, a novel chemical reaction representation learning model. Our model integrates the atomic correspondence between reactants and products, as well as information about the reaction center, enabling the model to better model the reaction process and gain a deeper understanding of the reaction mechanism. An adapter is utilized to incorporate reaction conditions, allowing our model to adapt to various modalities of reaction conditions and efficiently leverage previous work to enhance performance. Experimental results demonstrate that our model architecture outperforms existing reaction representation learning architectures across various downstream tasks. In the future, we plan to use this architecture for large-scale pretraining to use the reaction representation space to assist scientists in conducting research on reaction mechanisms.

Limitations. The model requires atom mappings as input. Although there are now tools for accurate atom-mapping, incorrect atom-mapping can still have a negative impact on the model’s performance. Like most deep-learning methods, our model requires a substantial amount of training data for support; hence, on small-scale datasets, our model still cannot surpass hand-crafted features.

References

- [1] Derek T Ahneman, Jesús G Estrada, Shishi Lin, Spencer D Dreher, and Abigail G Doyle. 2018. Predicting reaction performance in C–N cross-coupling using machine learning. *Science* 360, 6385 (2018), 186–190.
- [2] Mikhail Andronov, Varvara Voinarovska, Natalia Andronova, Michael Wand, Djork-Armé Clevert, and Jürgen Schmidhuber. 2023. Reagent prediction with a molecular transformer improves reaction data quality. *Chemical Science* 14, 12 (2023), 3235–3246.
- [3] Jimmy Lei Ba, Jamie Ryan Kiros, and Geoffrey E Hinton. 2016. Layer normalization. *arXiv preprint arXiv:1607.06450* (2016).
- [4] Jiayuan Chen, Kehan Guo, Zhen Liu, Olexandr Isayev, and Xiangliang Zhang. 2024. Uncertainty-Aware Yield Prediction with Multimodal Molecular Features. In *Proceedings of the AAAI Conference on Artificial Intelligence*, Vol. 38. 8274–8282.
- [5] Shuan Chen, Sunggi An, Ramil Babazade, and Yousung Jung. 2024. Precise atom-to-atom mapping for organic reactions via human-in-the-loop machine learning. *Nature Communications* 15, 1 (2024), 2250.
- [6] Tianqi Chen and Carlos Guestrin. 2016. Xgboost: A scalable tree boosting system. In *Proceedings of the 22nd acm sigkdd international conference on knowledge discovery and data mining*. 785–794.
- [7] Jacob Devlin, Ming-Wei Chang, Kenton Lee, and Kristina Toutanova. 2019. BERT: Pre-training of Deep Bidirectional Transformers for Language Understanding. In *Proceedings of the 2019 Conference of the North American Chapter of the Association for Computational Linguistics: Human Language Technologies, NAACL-HLT 2019, Minneapolis, MN, USA, June 2-7, 2019, Volume 1 (Long and Short Papers)*, Jill Burstein, Christy Doran, and Thamar Solorio (Eds.). Association for Computational Linguistics, 4171–4186. <https://doi.org/10.18653/V1/N19-1423>
- [8] Matthias Fey and Jan E. Lenssen. 2019. Fast Graph Representation Learning with PyTorch Geometric. In *ICLR Workshop on Representation Learning on Graphs and Manifolds*.
- [9] Shinsaku Fujita. 1986. Description of organic reactions based on imaginary transition structures. 1. Introduction of new concepts. *Journal of Chemical Information and Computer Sciences* 26, 4 (1986), 205–212.
- [10] Hanyu Gao, Thomas J. Struble, Connor W. Coley, Yuran Wang, William H. Green, and Klavs F. Jensen. 2018. Using Machine Learning to Predict Suitable Conditions for Organic Reactions. *ACS Central Science* 4 (11 2018), 1465–1476. Issue 11. <https://doi.org/10.1021/acscentsci.8b00357>
- [11] Jonathan Goodman. 2009. Computer software review: Reaxys.
- [12] Yanfei Guan, Connor W Coley, Haoyang Wu, Duminda Ranasinghe, Esther Heid, Thomas J Struble, Lagnajit Pattanaik, William H Green, and Klavs F Jensen. 2021. Regio-selectivity prediction with a machine-learned reaction representation and on-the-fly quantum mechanical descriptors. *Chemical science* 12, 6 (2021), 2198–2208.
- [13] Jongmin Han, Youngchun Kwon, Youn-Suk Choi, and Seokho Kang. 2024. Improving chemical reaction yield prediction using pre-trained graph neural networks. *Journal of Cheminformatics* 16, 1 (2024), 25.
- [14] Esther Heid, Kevin P. Greenman, Yunsie Chung, Shih-Cheng Li, David E. Graff, Florence H. Vermeire, Haoyang Wu, William H. Green, and Charles J. McGill. 2024. Chemprop: A Machine Learning Package for Chemical Property Prediction. *Journal of Chemical Information and Modeling* 64, 1 (2024), 9–17. <https://doi.org/10.1021/acs.jcim.3c01250> arXiv:<https://doi.org/10.1021/acs.jcim.3c01250> PMID: 38147829.
- [15] Weihua Hu, Matthias Fey, Marinka Zitnik, Yuxiao Dong, Hongyu Ren, Bowen Liu, Michele Catasta, and Jure Leskovec. 2020. Open graph benchmark: Datasets for machine learning on graphs. *Advances in neural information processing systems* 33 (2020), 22118–22133.
- [16] Weihua Hu, Bowen Liu, Joseph Gomes, Marinka Zitnik, Percy Liang, Vijay Pande, and Jure Leskovec. 2020. Strategies for Pre-training Graph Neural Networks. In *International Conference on Learning Representations*. <https://openreview.net/forum?id=HJlWWJFSFDH>
- [17] Ross Irwin, Spyridon Dimitriadis, Jiazhen He, and Esben Jannik Bjerrum. 2022. Chemformer: a pre-trained transformer for computational chemistry. *Machine Learning: Science and Technology* 3, 1 (2022), 015022.
- [18] Sho Ishida, Tomo Miyazaki, Yoshihiro Sugaya, and Shinichiro Omachi. 2021. Graph neural networks with multiple feature extraction paths for chemical property estimation. *Molecules* 26, 11 (2021), 3125.
- [19] Yuanfeng Ji, Lu Zhang, Jiayang Wu, Bingzhe Wu, Lanqing Li, Long-Kai Huang, Tingyang Xu, Yu Rong, Jie Ren, Ding Xue, et al. 2023. Drugood: Out-of-distribution dataset curator and benchmark for ai-aided drug discovery—a focus on affinity prediction problems with noise annotations. In *Proceedings of the AAAI Conference on Artificial Intelligence*, Vol. 37. 8023–8031.
- [20] Wengong Jin, Connor Coley, Regina Barzilay, and Tommi Jaakkola. 2017. Predicting organic reaction outcomes with weisfeiler-lehman network. *Advances in neural information processing systems* 30 (2017).
- [21] Yu-Ting Kao, Shu-Fen Wang, Meng-Hsiu Wu, Shwu-Huey Her, Yi-Hsuan Yang, Chung-Hsien Lee, Hsiao-Feng Lee, An-Rong Lee, Li-Chien Chang, and Li-Heng Pao. 2022. A substructure-based screening approach to uncover N-nitrosamines in drug substances. *Journal of Food & Drug Analysis* 30, 1 (2022).
- [22] Steven M Kearnes, Michael R Maser, Michael Wlekliński, Anton Kast, Abigail G Doyle, Spencer D Dreher, Joel M Hawkins, Klavs F Jensen, and Connor W Coley. 2021. The open reaction database. *Journal of the American Chemical Society* 143, 45 (2021), 18820–18826.

- [23] Angus Keto, Taicheng Guo, Morgan Underdue, Thijs Stuyver, Connor W. Coley, Xiangliang Zhang, Elizabeth H. Krenske, and Olaf Wiest. 2024. Data-Efficient, Chemistry-Aware Machine Learning Predictions of Diels–Alder Reaction Outcomes. *Journal of the American Chemical Society* (6 2024). <https://doi.org/10.1021/jacs.4c03131>
- [24] Sunghwan Kim, Jie Chen, Tiejun Cheng, Asta Gindulyte, Jia He, Siqian He, Qingliang Li, Benjamin A Shoemaker, Paul A Thiessen, Bo Yu, Leonid Zaslavsky, Jian Zhang, and Evan E Bolton. 2020. PubChem in 2021: new data content and improved web interfaces. *Nucleic Acids Research* 49, D1 (11 2020), D1388–D1395. <https://doi.org/10.1093/nar/gkaa971> arXiv:<https://academic.oup.com/nar/article-pdf/49/D1/D1388/35363961/gkaa971.pdf>
- [25] Diederik P Kingma and Jimmy Ba. 2014. Adam: A method for stochastic optimization. *arXiv preprint arXiv:1412.6980* (2014).
- [26] Youngchun Kwon, Dongseon Lee, Youn-Suk Choi, and Seokho Kang. 2022. Uncertainty-aware prediction of chemical reaction yields with graph neural networks. *Journal of Cheminformatics* 14 (2022), 1–10.
- [27] Greg Landrum et al. 2013. RDKit: A software suite for cheminformatics, computational chemistry, and predictive modeling. *Greg Landrum* 8 (2013), 31.
- [28] Pengyong Li, Jun Wang, Yixuan Qiao, Hao Chen, Yihuan Yu, Xiaojun Yao, Peng Gao, Guotong Xie, and Sen Song. 2021. An effective self-supervised framework for learning expressive molecular global representations to drug discovery. *Briefings in Bioinformatics* 22, 6 (2021), bbab109.
- [29] Shu-Wen Li, Li-Cheng Xu, Cheng Zhang, Shuo-Qing Zhang, and Xin Hong. 2023. Reaction performance prediction with an extrapolative and interpretable graph model based on chemical knowledge. *Nature Communications* 14, 1 (2023), 3569.
- [30] Xin Li, Shuo-Qing Zhang, Li-Cheng Xu, and Xin Hong. 2020. Predicting regioselectivity in radical C–H functionalization of heterocycles through machine learning. *Angewandte Chemie International Edition* 59, 32 (2020), 13253–13259.
- [31] Jieyu Lu and Yingkai Zhang. 2022. Unified deep learning model for multitask reaction predictions with explanation. *Journal of chemical information and modeling* 62, 6 (2022), 1376–1387.
- [32] Michael R Maser, Alexander Y Cui, Serim Ryou, Travis J DeLano, Yisong Yue, and Sarah E Reisman. 2021. Multilabel classification models for the prediction of cross-coupling reaction conditions. *Journal of Chemical Information and Modeling* 61, 1 (2021), 156–166.
- [33] John Mayfield, Daniel Lowe, and Roger Sayle. 2017. Pistachio: Search and faceting of large reaction databases. In *ABSTRACTS OF PAPERS OF THE AMERICAN CHEMICAL SOCIETY*, Vol. 254. AMER CHEMICAL SOC 1155 16TH ST, NW, WASHINGTON, DC 20036 USA.
- [34] Harry L Morgan. 1965. The generation of a unique machine description for chemical structures—a technique developed at chemical abstracts service. *Journal of chemical documentation* 5, 2 (1965), 107–113.
- [35] Chong Mou, Xintao Wang, Liangbin Xie, Yanze Wu, Jian Zhang, Zhongang Qi, and Ying Shan. 2024. T2i-adaptor: Learning adapters to dig out more controllable ability for text-to-image diffusion models. In *Proceedings of the AAAI Conference on Artificial Intelligence*, Vol. 38. 4296–4304.
- [36] Pratanphorn Nakliang, Sanghee Yoon, and Sun Choi. 2021. Emerging computational approaches for the study of regio- and stereoselectivity in organic synthesis. *Organic Chemistry Frontiers* 8, 18 (2021), 5165–5181.
- [37] Adam Paszke, Sam Gross, Francisco Massa, Adam Lerer, James Bradbury, Gregory Chanan, Trevor Killeen, Zeming Lin, Natalia Gimelshein, Luca Antiga, et al. 2019. Pytorch: An imperative style, high-performance deep learning library. *Advances in neural information processing systems* 32 (2019).
- [38] Daniel Probst, Philippe Schwaller, and Jean-Louis Reymond. 2022. Reaction Classification and Yield Prediction using the Differential Reaction Fingerprint DRFP. *Digital Discovery* (2022).
- [39] Yu Rong, Yatao Bian, Tingyang Xu, Weiyang Xie, Ying Wei, Wenbing Huang, and Junzhou Huang. 2020. Self-supervised graph transformer on large-scale molecular data. *Advances in neural information processing systems* 33 (2020), 12559–12571.
- [40] Mikolaj Sacha, Mikolaj Blaz, Piotr Byrski, Pawel Dabrowski-Tumanski, Mikolaj Chrominski, Rafal Loska, Pawel Wlodarczyk-Pruszyński, and Stanislaw Jastrzebski. 2021. Molecule edit graph attention network: modeling chemical reactions as sequences of graph edits. *Journal of Chemical Information and Modeling* 61, 7 (2021), 3273–3284.
- [41] Frederik Sandfort, Felix Strieth-Kalthoff, Marius Kühnemund, Christian Beecks, and Frank Glorius. 2020. A Structure-Based Platform for Predicting Chemical Reactivity. *Chem* 6, 6 (2020), 1379–1390. <https://doi.org/10.1016/j.chempr.2020.02.017>
- [42] Philippe Schwaller, Benjamin Hoover, Jean-Louis Reymond, Hendrik Strobel, and Teodoro Laino. 2021. Extraction of organic chemistry grammar from unsupervised learning of chemical reactions. *Science Advances* 7, 15 (2021), eabe4166.
- [43] Philippe Schwaller, Teodoro Laino, Théophile Gaudin, Peter Bolgar, Christopher A Hunter, Costas Bekas, and Alpha A Lee. 2019. Molecular transformer: a model for uncertainty-calibrated chemical reaction prediction. *ACS central science* 5, 9 (2019), 1572–1583.
- [44] Philippe Schwaller, Daniel Probst, Alain C Vaucher, Vishnu H Nair, David Kreutter, Teodoro Laino, and Jean-Louis Reymond. 2021. Mapping the space of chemical reactions using attention-based neural networks. *Nature Machine Intelligence* 3, 2 (2021), 144–152.
- [45] Philippe Schwaller, Alain C Vaucher, Teodoro Laino, and Jean-Louis Reymond. 2021. Prediction of chemical reaction yields using deep learning. *Machine learning: science and technology* 2, 1 (2021), 015016.
- [46] Jeffery I Seeman. 1986. The Curtin-Hammett principle and the Winstein-Holness equation: new definition and recent extensions to classical concepts. *Journal of Chemical Education* 63, 1 (1986), 42.
- [47] Runhan Shi, Gufeng Yu, Xiaohong Huo, and Yang Yang. 2024. Prediction of chemical reaction yields with large-scale multi-view pre-training. *Journal of Cheminformatics* 16, 1 (2024), 22.
- [48] Ashish Vaswani, Noam Shazeer, Niki Parmar, Jakob Uszkoreit, Llion Jones, Aidan N Gomez, Łukasz Kaiser, and Illia Polosukhin. 2017. Attention is all you need. *Advances in neural information processing systems* 30 (2017).
- [49] Petar Veličković, Guillem Cucurull, Arantxa Casanova, Adriana Romero, Pietro Liò, and Yoshua Bengio. 2018. Graph Attention Networks. In *International Conference on Learning Representations*.
- [50] Yue Wan, Chang-Yu Hsieh, Ben Liao, and Shengyu Zhang. 2022. Retroformer: Pushing the Limits of End-to-end Retrosynthesis Transformer. In *Proceedings of the 39th International Conference on Machine Learning (Proceedings of Machine Learning Research, Vol. 162)*, Kamalika Chaudhuri, Stefanie Jegelka, Le Song, Csaba Szepesvari, Gang Niu, and Sivan Sabato (Eds.). PMLR, 22475–22490. <https://proceedings.mlr.press/v162/wan22a.html>
- [51] Xiaorui Wang, Chang-Yu Hsieh, Xiaodan Yin, Jike Wang, Yuquan Li, Yafeng Deng, Dejun Jiang, Zhenxing Wu, Hongyan Du, Hongming Chen, Yun Li, Huanxiang Liu, Yuwei Wang, Pei Luo, Tingjun Hou, and Xiaojun Yao. 2023. Generic Interpretable Reaction Condition Predictions with Open Reaction Condition Datasets and Unsupervised Learning of Reaction Center. *Research* 6 (1 2023). <https://doi.org/10.34133/research.0231>
- [52] David Weininger. 1988. SMILES, a chemical language and information system. 1. Introduction to methodology and encoding rules. *Journal of chemical information and computer sciences* 28, 1 (1988), 31–36.
- [53] Chaochao Yan, Qianggang Ding, Peilin Zhao, Shuangjia Zheng, Jinyu Yang, Yang Yu, and Junzhou Huang. 2020. Retroxpert: Decompose retrosynthesis prediction like a chemist. *Advances in Neural Information Processing Systems* 33 (2020), 11248–11258.
- [54] Nianzu Yang, Kaipeng Zeng, Qitian Wu, Xiaosong Jia, and Junchi Yan. 2022. Learning substructure invariance for out-of-distribution molecular representations. *Advances in Neural Information Processing Systems* 35 (2022), 12964–12978.
- [55] Naruki Yoshikawa, Marta Skreta, Kourosh Darvish, Sebastian Arellano-Rubach, Zhi Ji, Lasse Bjørn Kristensen, Andrew Zou Li, Yuchi Zhao, Haoping Xu, Artur Kuramshin, et al. 2023. Large language models for chemistry robotics. *Autonomous Robots* 47, 8 (2023), 1057–1086.
- [56] Andrew F Zahrt, Jeremy J Henle, Brennan T Rose, Yang Wang, William T Darrow, and Scott E Denmark. 2019. Prediction of higher-selectivity catalysts by computer-driven workflow and machine learning. *Science* 363, 6424 (2019), eaau5631.
- [57] Kaipeng Zeng, Bo Yang, Xin Zhao, Yu Zhang, Fan Nie, Xiaokang Yang, Yaohui Jin, and Yanyan Xu. 2024. Ualign: pushing the limit of template-free retrosynthesis prediction with unsupervised SMILES alignment. *Journal of Cheminformatics* 16, 1 (2024), 80.
- [58] Lvmin Zhang, Anyi Rao, and Maneesh Agrawala. 2023. Adding conditional control to text-to-image diffusion models. In *Proceedings of the IEEE/CVF International Conference on Computer Vision*. 3836–3847.

A Statistical Information of Datasets

We summarize the statistical information of all the dataset set used in this work in Table 9.

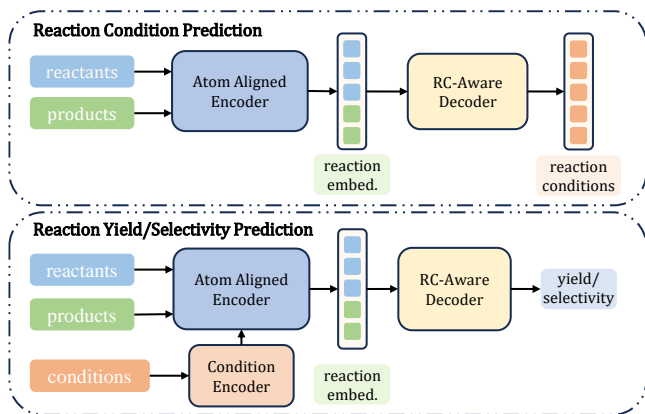
B Implementation Details

B.1 Pipeline for different tasks

This work does not train a multi-task unified model like T5chem [31]. Given the different datasets and varying inputs and outputs for each task, we have selected different modules to assemble the pipelines for the tasks discussed in this paper. The two pipelines involved are displayed in Fig. 2. The input for the reaction condition prediction task consists solely of reactants and products, hence the pipeline for this task is composed of an atom-aligned encoder followed by a RC-aware decoder with sequential output. For the reaction yield prediction and reaction selectivity prediction tasks, which also include reaction conditions in their input, we have incorporated a

Table 9: The statistical information of datasets in this work.

Dataset	Split-type	Train	Val	Test
USPTO_CONDITION	random split	544,591	68,075	68,075
USPTO_500MT	random split	116,360	12,937	14,238
Buchwald-Hartwig	random split	2,491	277	1187
	Test1	2,751	306	898
	Test2	2,749	306	900
	Test3	2,752	306	897
thiol addition	random split	677	75	323
	random split	3,851	428	1,835

**Figure 2: The pipelines for different tasks**

reaction condition encoder and utilized a RC-aware decoder with single output.

B.2 Initial node/edge feature extraction

We use the atom and bond encoder provided by Open Graph Benchmark [15]. These encoders transform the atom and chemical bonds into integer numbers based on their characteristics and molecular structure. Nine atom descriptors are provided, including the atom type, formal charge and other properties that can be calculated by RDKit [27]. As for chemical bonds, three descriptors are used, including bond type, bond stereochemistry as well as whether the bond is conjugated. Every descriptor corresponds to a learnable embedding table. The initial node and edge features are derived by aggregating the embeddings corresponding to each descriptor.

B.3 MPNN Layer in Atom Aligned Encoder

In contrast to many graphs where edges convey limited information, the chemical bonds within molecules play a pivotal role in determining their properties. Consequently, we employ a variant of the Graph Attention Network [49], akin to those utilized in the works of Yan et al. and Sacha et al., to integrate information from chemical bonds into the node features during the message-passing process. The MPNN layer we implement can be mathematically

formulated as follows:

$$\begin{aligned}
 \tilde{e}_{u,v} &= \text{FFN}_e(e_{u,v}), \\
 \tilde{h}_u &= \text{FFN}_n(h_u), \\
 c_{u,v} &= \mathbf{a}^T [\tilde{h}_u \parallel \tilde{h}_v \parallel \tilde{e}_{u,v}], \\
 \alpha_{u,v} &= \frac{\exp(\text{LeakyReLU}(c_{u,v}))}{\sum_{v' \in \mathcal{N}(u) \cup \{u\}} \exp(\text{LeakyReLU}(c_{u,v'}))}, \\
 h'_u &= \sum_{v \in \mathcal{N}(u) \cup \{u\}} \alpha_{u,v} (\tilde{h}_u + \tilde{e}_{u,v}^{(k)}),
 \end{aligned} \tag{8}$$

where h_u represents the input node feature of node u , $e_{u,v}$ represents the input edge feature of edge (u, v) and h'_u represents the output node feature of u of the message passing layer.

B.4 Condition Encoders for Buchwald–Hartwig and thiol addition Selectivity Dataset

The Buchwald–Hartwig and thiol addition selectivity dataset uses chemical reagents as reaction conditions. To generate condition features, we employ a graph neural network. It should be noted that the number of distinct reagents in these datasets is quite limited, with less than 50 different molecules available, which makes it challenging to train a reaction condition encoder from scratch. Therefore, we have opted to use a pretrained molecular representation model proposed by Hu et al. This model is lightweight and has been pretrained using only the random atom masking task. The roll-out form of the k -th layer of this model is formulated as

$$\begin{aligned}
 X &= \sum_{u \in \mathcal{N}(v) \cup \{v\}} h_u^{(k-1)} + \sum_{e=(u,v)} \sum_{u \in \mathcal{N}(v) \cup \{v\}} h_e^{(k-1)}, \\
 h_v^{(k)} &= \text{ReLU}(\text{MLP}^{(k)}(X)),
 \end{aligned} \tag{9}$$

where $h_u^{(k)}$ is the node feature of node u in k -th layer and $h_e^{(k)}$ is the edge feature of edge e in k -th layer. Using this pretrained model does not compromise the fairness of our experiments, as our compared baselines are also pretrained on chemical reaction datasets. Moreover, this further illustrates that our design can efficiently integrate existing works for chemical reaction representation learning, even if these works were not specifically designed for chemical reactions.

B.5 Model Implementation details

We implement our model based on torch_geometric 2.2.0 [8] and Pytorch 1.13 [37]. For model for reaction condition prediction, we set the hidden size as 512, encoder layer as 6, decoder layer as 6 and the number of attention heads as 8. The dropout ratio is set as 0.1. The highest learning rate of each model as set as 1.25e-4. We slowly increase our learning rate to the highest in the first few epochs and slowly decrease it using exponential decay. For reaction yield prediction, we set the hidden size as 128, encoder layers as 3 and attention heads as 8. The dropout ratio is set as 0.1 and the learning rate is set as 1e-4. For reaction selectivity prediction in Thiol addition dataset, we set the hidden size as 128, encoder layers as 3 and attention heads as 8. The dropout ratio is set as 0.0 and the learning rate is set as 5e-5. For reaction selectivity prediction in C-H functionalization dataset, we set the hidden size as 128, encoder layers as 5 and attention heads as 8. The dropout ratio is set as 0.0

and the learning rate is set as $5e-4$. All models are trained with Adam optimizer [25]. We will consider open-sourcing our code upon the paper acceptance.

C Data Preparation

C.1 Adding Atom-mapping

The Buchwald-Hartwig dataset features a consistent reaction template across all its reaction data, enabling the derivation of atom-mapping through rule-based approaches. For all the other datasets except the Buchwald-Hartwig dataset, we have employed Rxnmapper [42] to obtain atom-mapping. It is noteworthy that we have re-annotated the labels for the USPTO_500MT dataset, treating both the originally provided reactants and reagents as input reactants during the atom mapping annotation for this dataset. For further details on the processing of the USPTO_500MT dataset, please refer to Appendix C.2.

C.2 Generation of Reagents of USPTO_500MT

We restructured our dataset. Following the annotations provided by the dataset, we divided the reactants involved in the reactions into a series of charge-balanced ions or molecular clusters. Here, we treat a cluster as a single molecule, rather than segmenting molecules based on the delimiter ':' as in prior studies. Utilizing RXNMapper [42], we appended atom-mapping to the reactions, where molecules in the original reactants that have atoms present in the products are considered reactants, and the remaining portions

are classified as reagents. We categorized the reagents according to the following hierarchy:

- If a molecule is a free metal, or it contains a cyclic structure along with a metal or phosphorus atom, or it is a metal halide, it is designated as Type I.
- If a molecule is an organic compound, it is designated as Type II.
- The remaining molecules are categorized as Type III.

Our data labels are constructed in the order of Type I, Type II, and Type III. When reagents contain multiple molecules of the same type, these molecules are sorted in ascending order of their SMILES string lengths within the same category.

D Further elaboration on reaction condition prediction

To provide a more detailed exposition of the input, output, and evaluation metrics for the reaction condition prediction task, we present several examples in Fig. 3 and Fig. 4. In the USPTO_CONDITION dataset, a reaction condition is defined by the presence of a catalyst, reagent, and solvent. A reaction condition combination is deemed correct if all components are accurately predicted, with a component being considered correctly predicted only if every molecule within it is predicted without error. Conversely, for the USPTO_500MT dataset, which does not classify reaction conditions further, a prediction is deemed correct if the predicted molecules match exactly with those in the labeled data.

Reaction	Catalyst	Solvent	Reagent
	Ground truth:		
	Prediction:		 X Pyridine is predicted into Triethylamine, wrong reagent (X)
	Ground truth:		
	Prediction:		(checkmark)

Figure 3: A example of correct and wrong predictions for USPTO_CONDITION dataset.

Reaction	Ground Truth	Prediction
		 X Trifluoroacetic acid is predicted into Methanol (X)
		 X Dimethylformamide is erroneously predicted (X)
		(checkmark)

Figure 4: A example of correct and wrong predictions for USPTO_500MT dataset.